

Postcollision-interaction effects in multistep Auger transitions following Ar 1s photoionization

S. Kosugi,^{1,2} R. Guillemin,³ O. Travnikova^{3,4}, T. Marchenko^{3,4}, D. Koulentianos^{3,*}, J. B. Martins^{3,†}, F. Hosseini,³ R. Püttner⁵, D. Céolin,⁴ L. Journal^{3,4}, M. N. Piancastelli^{3,6}, I. Ismail,^{3,4} F. Koike,¹ M. Iizawa⁷, S. Sheinerman⁸, L. Gerchikov⁹, Y. Azuma^{1,10,‡} and M. Simon^{3,4}

¹Department of Materials and Life Sciences, Sophia University, Tokyo 102-8554, Japan

²Department of Physics, Tokyo Gakugei University, Tokyo 184-8501, Japan

³Sorbonne Université, CNRS, UMR 7614, Laboratoire de Chimie Physique-Matière et Rayonnement, F-75005 Paris, France

⁴Synchrotron SOLEIL, l'Orme des Merisiers, Saint-Aubin, BP 48, F-91192 Gif-sur-Yvette Cedex, France

⁵Fachbereich Physik, Freie Universität Berlin, Arnimallee 14, D-14195 Berlin, Germany

⁶Department of Physics and Astronomy, Uppsala University, Box 516, SE-75120 Uppsala, Sweden

⁷Department of Physics, Rikkyo University, Tokyo 171-8501, Japan

⁸Department of Physics, St. Petersburg State Marine Technical University, 190121 St. Petersburg, Russia

⁹Department of Physics, Peter the Great St. Petersburg Polytechnic University, 195251 St. Petersburg, Russia

¹⁰Department of Physics, Indian Institute of Technology Delhi, Hauz Khas, New Delhi 110016, India



(Received 10 March 2022; accepted 18 August 2022; published 23 September 2022)

Postcollision-interaction (PCI) effects involving multistep decay processes following Ar 1s photoionization has been studied by Auger electron spectroscopy. The experiment focused on *LMM* Auger electrons measured in small photon energy steps across the Ar 1s photoionization threshold. Decay pathways that we studied include (1) the $\text{Ar}^{2+}2p^{-1} \rightarrow \text{Ar}^{2+}3p^{-2}$ *LMM* α Auger process due to a single *L* hole created by *KL* fluorescence, (2) the $\text{Ar}^{2+}2p^{-2} \rightarrow \text{Ar}^{3+}2p^{-1}3p^{-2}$ *LMM* $_1$ Auger process following double *L* shell hole states produced by a *KLL* Auger processes, and (3) the subsequent $\text{Ar}^{3+}2p^{-1}3p^{-2} \rightarrow \text{Ar}^{4+}3p^{-4}$ *LMM* $_2$ Auger transitions. Particularly pronounced PCI shifts and unusual line shapes compared to the ordinary one-step PCI process were found in the spectra of Auger processes following a *KLL* Auger first step. The experimental results were compared with calculations based on the semiclassical approach to PCI. Good agreement was found between the calculated and experimental PCI shifts. The result opens possibilities for further studies of the multielectron dynamics between Auger electrons mediated through the photoelectron in these and similar systems.

DOI: [10.1103/PhysRevA.106.033114](https://doi.org/10.1103/PhysRevA.106.033114)

I. INTRODUCTION

Numerous studies have been conducted so far on postcollision-interaction (PCI) effects taking place upon photoionization close to an inner-shell ionization threshold [1–47]. Energy exchange takes place between the photoelectron and the faster Auger electron produced by the subsequent inner-shell relaxation process. In the classical picture, PCI can be understood as due to the change in the Coulomb potential felt by the Auger electron and the photoelectron upon the takeover. Experimental investigations of the PCI effects were conducted more with the photoelectron spectra rather than with the Auger electron spectrum. In the case of single Auger decay, the PCI distortion and shift of the Auger electron peak merely mirrors the PCI distortion and shift of the photoelectron peak following the energy conservation law.

However, for inner-shell photoionization, PCI involved in the cascade decay steps including fluorescence as well as multiple Auger electrons subsequently emitted through the relaxation process have to be considered. Close to the photoionization threshold, the photoelectron is taken over by all of the Auger electrons one after another, and thus gets affected by all of them. On the other hand, each Auger electron line is affected only by its particular takeover interaction with the photoelectron.

The aim of this study is to reveal and compare the influence of PCI on each of the Auger electrons following the inner-vacancy decay. The PCI effects in the photoionization of inner shells accompanied by sequential double Auger (DA) or multiple Auger processes have so far been investigated by several coincidence methods. Threshold electron/residual ions coincidence was utilized for the investigation of the threshold photoelectron yield in the vicinity of inner vacancies in Kr, Ar, and Xe [36,38–44]. The method of threshold electron/Auger electron coincidences was applied to the investigation of 4*d* threshold photoelectrons in Xe [45,46]. Multielectron coincidence methods were used to investigate the photoelectron spectra distorted by DA decay in Ar and Kr [22,32,33]. Subsequently, coincidences between the slow photoelectron and the residual ions were used to study the PCI effects in the photoelectron spectra distorted

*Present address: Center for Free-Electron Laser Science & Department of Physics, Universität Hamburg, Luruper Chaussee 149, 22761 Hamburg, Germany.

†Present address: X-ray Science Division, Argonne National Laboratory, Lemont, IL 60439, USA.

‡y-azuma@sophia.ac.jp

by DA and multiple Auger decay in Ar and the molecule carbonyl sulfide (OCS) [34,47].

On the theoretical side, models were presented for PCI associated with few Auger electron decay as follows: a classical model to describe the release of threshold electrons in the DA process [43], a classical model of cascade Auger decay [36], a time-dependent quantum mechanical model for cascade Auger processes [29], a quantum mechanical eikonal approach to the direct DA and cascade DA processes (DDA and CDA, correspondingly) [1,13], and a semiclassical approach to the DDA and CDA processes [19].

Progress was made on the differentiation of the decay pathways by Guillemin *et al.* [34] with photoelectron-ion coincidence measurements on Ar $1s$ photoionization. They succeeded in measuring PCI effects on the photoelectron specific to each final ion charge state and compared them with theoretical calculations. Their result could distinguish PCI effects due to different subsets of cascade pathways leading to a particular final ion charge. Nevertheless, the relaxation steps within the cascade pathways could not be differentiated since the photoelectrons only manifested the cumulative result after all takeover events of the multiple Auger electrons leading to a particular final ion charge. Then, Guillemin *et al.* [35] examined the PCI effect on the KLL Auger electron ejected by the first step in the Auger cascade of Ar and obtained experimental results in good agreement with the ordinary one-step PCI model. Arp *et al.* [37] conducted coincidence measurements between KL fluorescence and LMM Auger electrons to study the PCI between $1s$ photoelectron and LMM Auger after KL fluorescence.

Overall, considerable efforts have been made so far in the investigation ranging from threshold or slow photoelectron spectra to limited results concerning the first step Auger electron. However, the PCI influence on Auger electrons beyond the first KLL Auger step has not been investigated in any experimental or theoretical approaches.

We present the investigation of the PCI distortion and shift experienced by cascade Auger electrons following $1s$ photoionization of Ar. Two types of pathways for the relaxation of Ar immediately following $1s$ photoionization are considered. One of them starts with the KL (or KM) fluorescence emission filling the K vacancy. The KL fluorescence would result in the creation of a L hole which would be followed by a further subsequent Auger process. In another case, the Auger process (KLL , KLM) can fill the initial K shell hole and create double vacancies that can in turn get filled in by subsequent Auger processes.

Three different regions in the Auger spectrum were selected for our study: $LMM\alpha$, LMM_1 , and LMM_2 , that can be attributed respectively to single Auger, cascade DA, and further multiple Auger processes. All three lines show significant shifts and characteristic line shapes caused by the PCI. Our measurements have been compared to our calculation performed within the framework of the existing semiclassical approximations [7,19]. Good agreement of measured and calculated shifts demonstrates the reliability of the results obtained and underscores the importance of PCI effects in the analysis of the cascade Auger lines after inner-shell photoionization near threshold.

This paper is organized as follows. Section II presents a brief description of our experimental method. Section III presents the analysis of the processes considered and the theoretical approach for calculation of the cross section of the single Auger and cascade double Auger processes. In Sec. IV we present the analysis and comparison of our measurements with calculation. The atomic unit system with $|e| = m_e = \hbar = 1$ is used throughout.

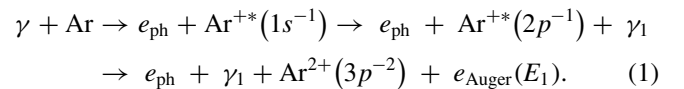
II. EXPERIMENT

The experiment was conducted at the x-ray beamline GALAXIES at the SOLEIL synchrotron. Linearly polarized light was generated by the U20 undulator and monochromatized with a Si double crystal monochromator [48]. Light was then passed through a gas cell and the emitted electrons were measured with a hemispherical analyzer (Scienta EW4000) whose lens axis was set parallel to the linear polarization of the photon [49]. At 3.2 keV, the photon energy bandwidth was approximately 350 meV. The total resolution of the hemispherical analyzer was 180 meV with pass energy 100 eV. The photon energy was calibrated by utilizing the Ar $1s^{-1}4p$ resonance (3203.5 eV) [50].

III. THEORETICAL DESCRIPTION OF PROCESSES INVOLVING LMM AUGER TRANSITIONS

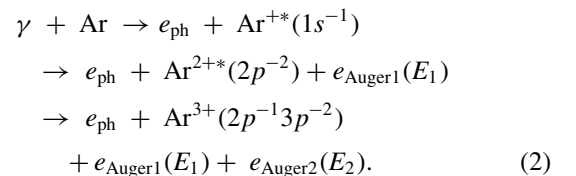
A. Processes

The LMM Auger lines can result from cascade processes that occur in two or several steps. The $LMM\alpha$ Auger electrons are produced by a two-step cascade process [34,51]. Initially a photoelectron is emitted from the K shell and the inner $1s^{-1}$ vacancy is created. After that, radiative decay of the $1s^{-1}$ vacancy happens as the first step of the cascade process and a $2p^{-1}$ vacancy is created in the intermediate shell. An Auger decay of this vacancy leads to the creation of two holes in the outer $3p^6$ shell and the emission of $LMM\alpha$ Auger electrons with energies E_1 close to 200 eV. This process can be written as

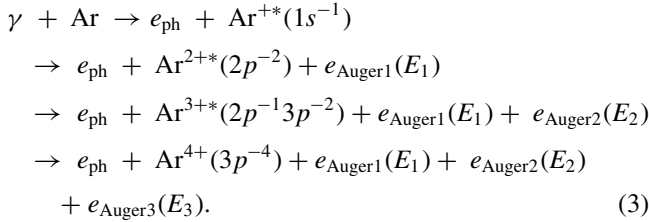


The LMM_1 Auger electrons are emitted in the sequential double Auger decay of the inner $1s^{-1}$ vacancy. In the first step of this decay process the fast Auger electron with energy E_1 close to 2660 eV is emitted and the two-hole state in the intermediate $2p^6$ shell is created. The second Auger decay of this state leads to an emission of the LMM_1 Auger electron with energy E_2 close to 220 eV and the creation of the three-hole state $2p^{-1}3p^{-2}$ of the residual ion.

This decay process can be written as



The LMM_2 Auger electrons are emitted in a multiple cascade Auger decay of the inner $1s^{-1}$ vacancy. The first step of this cascade is a transition $1s^{-1} \rightarrow 2p^{-2}$ and the emission of a fast Auger electron with energy $E_1 = 2660$ eV. The second step is a transition $2p^{-2} \rightarrow 2p^{-1}3p^{-2}$ and an emission of the second Auger electron with energy $E_2 \approx 220$ eV. The final step is a transition $2p^{-1}3p^{-2} \rightarrow 3p^{-4}$ and an emission of the LMM_2 Auger electron with energy $E_3 \approx 180$ eV. This decay process can be written as



In each considered processes (1)–(3) all emitted electrons are affected by the PCI which has to be taken into account at an analysis of the measured electron's spectra.

B. PCI on the $LMM\alpha$ Auger electrons

The $LMM\alpha$ Auger electrons in the process (1) are emitted in the two-step cascade process. The first step of this cascade is the radiative decay of the $1s^{-1}$ vacancy which does not change the charge state of the ion. Hence the emitted photoelectron “feels” the field of a singly charged ion before the Auger decay (the second step of the cascade) and the field of a doubly charged ion after the Auger decay. Consequently, the PCI effects in the process (1) are similar to those in the inner-shell photoionization process followed by a single Auger decay. In such a process the PCI manifest itself as the interaction of the slow photoelectron with the field of the singly charged ion before the Auger decay and with the field of the doubly charged ion after the Auger decay as well as the interaction between the photoelectron and Auger electron. Within the quantum mechanical approach there are several models that take this interaction into account [3,7,8,18]. We will use a semiclassical approximation [7] which correctly describes the PCI effects in the near-threshold region that corresponds to the region of measurements. This approach allows us to calculate the line shape of the emitted photoelectrons and the mirror-reflected profile of the Auger electrons. In this approach, the amplitude A_{SA} of the photoionization process occurring via single Auger decay of the inner vacancy is presented as an overlap integral,

$$A_{SA} = M \langle \psi_f | \psi_i \rangle, \tag{4}$$

between the photoelectron wave functions in the intermediate ψ_i and final ψ_f states. The photoelectron in the intermediate state moves in the field of the singly charged metastable ion with complex energy $\Delta E + i\Gamma/2$ where ΔE is the excess of photon energy above the photoionization threshold and Γ is the inner vacancy width. The wave function of the final photoelectron state ψ_f describes propagation of the outgoing photoelectron with the energy E_{ph} in the field of the doubly charged ion and the emitted Auger electron with the energy E_1 . The factor M which slowly depends on the emitted electrons energies E_{ph} and E_1 contains amplitudes of

the photoionization and the Auger decay. Thus, the electron emission energy profile is primarily determined by the wavefunction overlap integral in Eq. (4). In the case of weak PCI, e.g., at a very high excess energies ΔE , squared overlap integral $|\langle \psi_f | \psi_i \rangle|^2$ gives the Lorentzian line shape of the width Γ centered for photoelectron spectrum at $E_{\text{ph}} = E_{\text{ph}}^{(0)} = \Delta E$ and for Auger electron spectrum at unshifted Auger energy value $E_1 = E_1^{(0)}$. With decrease of the excess energy ΔE the photoelectron velocity also decreases. Consequently, the distance between the photoelectron and the ion on the moment of the Auger decay decreases and therefore the PCI strengthens. It leads to the distortion of energy distributions resulting in a shift decreasing the energy of the photoelectron line maximum by $\varepsilon_{\text{ph}} = E_{\text{ph}} - E_{\text{ph}}^{(0)} < 0$. This energy lost by the photoelectron is transmitted to the Auger electron whose energy of the line maximum shifts toward higher energy by $\varepsilon_1 = E_1 - E_1^{(0)} = -\varepsilon_{\text{ph}}$.

Within the semiclassical approach, the photoelectron wave functions are considered in the approximation of Wentzel, Kramers, and Brillouin (WKB functions) and the evaluation of the overlap integral is carried out by the saddle point method. For the details of evaluation and final result see, e.g., Refs. [7,19].

The photoionization process (1) where $1s^{-1}$ vacancy decays via a cascade process starting from fluorescence is more complicated than the single Auger process described above following the model of Ref. [7]. However, the first cascade step, the radiative decay of the $1s^{-1}$ vacancy, does not change the ionic charge. The emitted photoelectron moves in the field of the singly charged ion during the effective time $\tau_{\text{eff}} = \tau_{1s} + \tau_{2p}$, where τ_{1s} and τ_{2p} are the lifetimes of the $1s^{-1}$ and $2p^{-1}$ vacancies, respectively. Then the Auger decay occurs resulting in the PCI energy exchange between the photoelectron and the Auger electron. It is similar to the single Auger decay process with the change of time delay between the ionization and the Auger decay events from τ_{1s} to τ_{eff} . Consequently, applying the model [7] to the process (1) we have to use the effective width of the inner vacancy $\Gamma_{\text{eff}} = \Gamma_{1s}\Gamma_{2p}/(\Gamma_{1s} + \Gamma_{2p})$. Such an approach was used earlier to study the PCI distorted photoelectron spectra [34,47] and its applicability was shown. Using the values $\Gamma_{1s} = 690$ meV [52] and $\Gamma_{2p} = 118$ meV [53] we have obtained the effective lifetime width $\Gamma_{\text{eff}} = 101$ meV.

C. PCI on the LMM_1 Auger electrons

The LMM_1 Auger electrons are emitted in the second step of the cascade Auger decay starting from the $1s$ vacancy [process (2)]. There are a few approaches within the quantum mechanical framework to consider the PCI effects in the cascade Auger processes: the eikonal approach [1], the semiclassical approach [19], and the time-dependent approach [29]. The first two [1,19] would allow the calculation of the energy distributions of the emitted Auger electrons, but the eikonal approach [1] has restrictions that do not allow its use in the near-threshold region. Hence, for consideration of the PCI influence on the Auger electron line shapes for small excess photon energies above threshold, we used the semiclassical approach [19]. This theory has been successfully applied

earlier for the description of the PCI distortion of the slow photoelectron spectra [19,22,34,47].

According to the semiclassical approach [19] the amplitude A_{CDA} of the cascade double Auger decay process (2) is given by an integral over the intermediate photoelectron energy E'_{ch} of the product of the two amplitudes, $I_{\text{ph}}(E'_{\text{ch}})$ and $I_A(E'_{\text{ch}})$, which describe the propagation of the photoelectron and the first Auger electron, respectively:

$$A_{\text{CDA}} = \int_{-\infty}^{\infty} I_{\text{ph}}(E'_{\text{ch}}) I_A(E'_{\text{ch}}) \frac{dE'_{\text{ch}}}{2\pi}. \quad (5)$$

The photoelectron in the course of the cascade double Auger decay process (2) undergoes two consecutive shakes at the moments of Auger decays. Consequently, its amplitude is given by the product of two overlap integrals between photoelectron wave functions,

$$I_{\text{ph}}(E'_{\text{ch}}) = M_{\text{ph}} \langle \psi_f | \psi_{E'_{\text{ch}}} \rangle \langle \psi_{E'_{\text{ch}}} | \psi_i \rangle. \quad (6)$$

Here the photoionization amplitude M_{ph} varies slowly with the electron energy. The shake-off amplitude of the first Auger decay is given by the overlap integral $\langle \psi_{E'_{\text{ch}}} | \psi_i \rangle$ between the photoelectron wave functions of two intermediate photoelectron states. The wave function ψ_i is the same as in the A_{SA} amplitude (4). It describes the photoelectron motion with complex energy $\Delta E + i\Gamma_{1s}/2$ in the field of the singly charged metastable ion $\text{Ar}^{+*}(1s^{-1})$ prior to the first Auger decay. The wave function $\psi_{E'_{\text{ch}}}$ describes the photoelectron motion with energy E'_{ch} in the field of the doubly charged ion $\text{Ar}^{2+*}(2p^{-2})$ and the first Auger electron between two Auger decays. The shake-off amplitude of the second Auger decay is given by the overlap integral $\langle \psi_f | \psi_{E'_{\text{ch}}} \rangle$ between the intermediate photoelectron wave function $\psi_{E'_{\text{ch}}}$ and the wave function ψ_f of the final photoelectron state with the energy $E_{\text{ph}} = E_{\text{ph}}^{(0)} + \varepsilon_{\text{ph}}$ in the field of residual ion $\text{Ar}^{3+*}(2p^{-1}3p^{-2})$ and two Auger electrons.

The Auger electron amplitude $I_A(E'_{\text{ch}})$ is given by the product

$$I_A(E'_{\text{ch}}) = M_1 M_2 \langle \psi_{E_1} | \psi_{E'_1} \rangle \quad (7)$$

of the amplitudes of the first, M_1 , and the second, M_2 , Auger decays and the overlap integral $\langle \psi_{E_1} | \psi_{E'_1} \rangle$ of the first Auger electron wave functions. This overlap integral presents the shake-off amplitude at the moment of the second Auger decay. The function $\psi_{E'_1}$ is the wave function of the first Auger electron with complex energy $E'_1 = E_1^{(0)} - E'_{\text{ch}} + \Delta E + i\Gamma_{2p^2}/2$ moving in the field of the doubly charged ion $\text{Ar}^{2+*}(2p^{-2})$ and the photoelectron prior to the second Auger decay. The wave function ψ_{E_1} describes the first Auger electron motion with its final energy E_1 in the field of residual ion $\text{Ar}^{3+*}(2p^{-1}3p^{-2})$, the outgoing photoelectron, and the second Auger electron.

Intermediate states of the photoelectron $\psi_{E'_{\text{ch}}}$ and the first Auger electron $\psi_{E'_1}$ between two Auger decays are virtual. That is why the amplitude A_{CDA} is evaluated by integration over their energies in Eq. (5). Note here that the Auger amplitude I_A depends on the photoelectron energy E'_{ch} via the first Auger electron energy in the intermediate state, E'_1 , which is connected with photoelectron energy by the energy conservation $E'_1 = E_1^{(0)} - E'_{\text{ch}} + \Delta E + i\Gamma_{2p^2}/2$. Note also that the

amplitude A_{CDA} depends on the widths $\Gamma_1 = \Gamma_{1s}$ and $\Gamma_2 = \Gamma_{2p}$ of the intermediate states involved.

All electronic wave functions in the overlap integrals in amplitudes I_{ph} and I_A have been taken in the WKB approximation. Their explicit forms as well as the evaluation details are presented in Ref. [19]. The electronic wave functions in the region of negative energies are obtained by analytical continuation. The evaluation of the overlap integrals (6) and (7) was carried out by the saddle point method. The integration over the energy E'_{ch} in Eq. (5) was performed numerically. Subsequent to that, the cross section of the process (2) was obtained by squaring the modulus of Eq. (5),

$$\frac{d^2\sigma}{d\varepsilon_{\text{ph}} d\varepsilon_2} = |A_{\text{CDA}}(E_{\text{ph}}, E_1, E_2)|^2. \quad (8)$$

Here, ε_{ph} and ε_2 are the energies of the photoelectron and the second Auger electron measured relative to their unshifted values $E_{\text{ph}}^{(0)}$ and $E_2^{(0)}$: $\varepsilon_{\text{ph}} = E_{\text{ph}} - E_{\text{ph}}^{(0)}$ and $\varepsilon_2 = E_2 - E_2^{(0)}$.

Note that due to energy conservation, $\varepsilon_{\text{ph}} + \varepsilon_1 + \varepsilon_2 = 0$, there are only two independent energies ε_i . The energy distribution of the second Auger electron can be obtained by the integration of the cross section (8) over the energy of the photoelectron ε_{ph} or the first Auger electron ε_1 within the limits of the line profile:

$$\frac{d\sigma}{d\varepsilon_2} = \int_{E_{1l}}^{E_{1h}} |A_{\text{CDA}}(E_{\text{ph}}, E_1, E_2)|^2 d\varepsilon_1. \quad (9)$$

D. PCI on the LMM_2 Auger electrons

The LMM_2 Auger electrons are emitted in the third step of the multiple cascade Auger decay of the $1s$ vacancy [see process (3)]. To the best of our knowledge there has been no exact theory that describes the PCI influence on the Auger electrons emitted in multiple Auger decays. However, we can try to estimate this influence with some approximations. Our approximation is based on the following assumptions: (i) The LMM_2 Auger electron, $e_{\text{Auger}3}(E_3)$, is emitted with energy E_3 , which is lower than the energies of the preceding $e_{\text{Auger}1}(E_1)$ and $e_{\text{Auger}2}(E_2)$ Auger electrons ($E_1 \sim 2660$ eV, $E_2 \sim 220$ eV, and $E_3 \sim 180$ eV in our case). This emission occurs when the electrons $e_{\text{Auger}1}$ and $e_{\text{Auger}2}$ are located far from the residual ion. Hence the contribution to the PCI shift of the LMM_2 Auger line from the interaction with the Auger electrons from earlier steps is small compared to the interaction of the $e_{\text{Auger}3}$ Auger electron with the slow photoelectron and the residual ion. Such an assumption is more valid for the $e_{\text{Auger}1}/e_{\text{Auger}3}$ interaction than for the $e_{\text{Auger}2}/e_{\text{Auger}3}$ one. The numerical estimation for the case of the two-step sequential Auger process shows that neglecting the interaction between the 180 eV and 220 eV Auger electrons leads to an error of up to 20% in the value of the Auger electron shift. (ii) The main contribution to the $e_{\text{Auger}3}$ electron shift comes from the energy exchange between the photoelectron and the $e_{\text{Auger}3}$ electron which in turn occurs due to the shake process upon the change of the ionic charge state at the moment of the LMM_2 Auger transition. (iii) By taking into account only this main contribution to the PCI energy shift we reduce the complicated PCI problem for five charged particles to the well known PCI problem of single

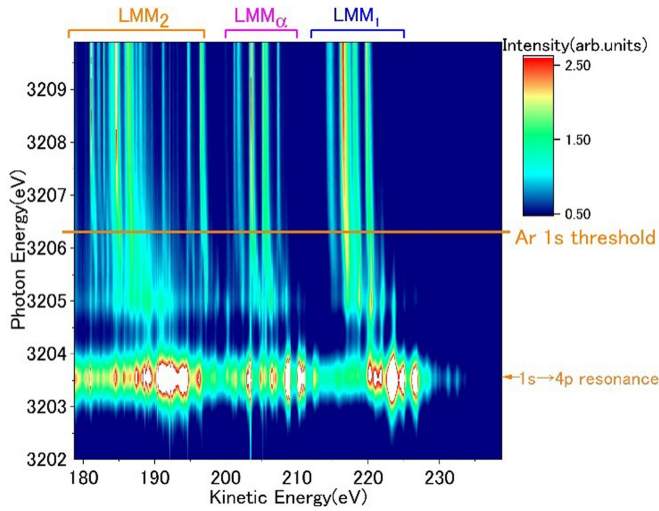


FIG. 1. Two-dimensional (2D) overview map of the Auger electron spectra with electron kinetic energies approximately 180–240 eV and photon energies 3202.0–3209.9 eV.

Auger decay involving one Auger electron, photoelectron, and residual ion. Within this approximation we will use the PCI energy shift ε of the single Auger decay process to estimate the PCI energy shift ε_3 of the third Auger electron in the cascade Auger decay process (3). We will employ a simple equation for the PCI energy shift ε of the single Auger decay process obtained within the semiclassical approximation [9],

$$\Gamma\sqrt{2(\Delta E + \varepsilon)} - 4\varepsilon(\Delta E + \varepsilon) - \varepsilon^2 = 0. \quad (10)$$

In order to adapt this equation for process (3) we need to introduce some modifications. The PCI energy shift is actually determined by the position of the slow photoelectron at the moment of Auger decay. In the case of single Auger decay the photoelectron undergoes the shake-off when it is located at a distance $r \sim V_{\text{ph}}\tau$ from the ion. Here, V_{ph} denotes the photoelectron velocity and $\tau = 1/\Gamma$ is the Auger decay time. In process (3) the slow photoelectron at the moment of the third Auger decay is located at a distance $r \sim V_{\text{ph}}(\tau_{1s} + \tau_{2p^2} + \tau_{2p})$ from the ion, where τ_{1s} , τ_{2p^2} , τ_{2p} are the lifetimes of intermediate states $\text{Ar}^{+*}(1s^{-1})$, $\text{Ar}^{2+*}(2p^{-2})$, and $\text{Ar}^{3+*}(2p^{-1}3p^{-2})$ of the Ar ion, respectively. Using Eq. (10) for ε_3 estimation with $\Gamma = \Gamma_{2p} = 1/\tau_{2p}$, we have to scale the photoelectron velocity as $V_{\text{eff}} = V_{\text{ph}}(\tau_{1s} + \tau_{2p^2} + \tau_{2p})/\tau_{2p}$ in order to make the photoelectron distance equal to $r \sim V_{\text{eff}}\tau_{2p} = V_{\text{ph}}(\tau_{1s} + \tau_{2p^2} + \tau_{2p})$. Consequently, the excess photon energy $\Delta E = V_{\text{ph}}^2/2$ should be scaled as $\Delta E_{\text{eff}} = \Delta E(\tau_{1s} + \tau_{2p^2} + \tau_{2p})^2/\tau_{2p}^2$. With this modification of the excess energy, Eq. (10) with the vacancy width of $\Gamma = \Gamma_{2p}$ can be used to estimate the LMM_2 Auger line shift.

IV. RESULTS AND DISCUSSION

The two-dimensional (2D) map of the Auger electron spectra with electron energies of approximately 180–240 eV and photon energies 3202.0–3209.9 eV is shown in Fig. 1. The assignment of the peaks in the spectra was accomplished based on previous LMM line measurements with photon energies well above the $1s$ threshold (3206.3 eV [54]) by Werme *et al.*

[55], Bush *et al.* [56], and Guillemin *et al.* [57]. Three different energy regions corresponding to different LMM processes, $LMM\alpha$, LMM_1 , and LMM_2 , can be distinguished. At photon energies above the Ar $1s$ threshold energy, the $2p^{-1} \rightarrow 3p^{-2}$ LMM spectrum following KL fluorescence ($LMM\alpha$) was found in the electron energy region 200–210 eV [57]. In the 210–235 eV electron energy region, $2p^{-2} \rightarrow 2p^{-1}3p^{-2}$ Auger electrons from the double L hole state following KLL Auger process (LMM_1) were found [57]. In the electron energy region 175–200 eV, peaks due to the $2p^{-1}3p^{-2} \rightarrow 3p^{-4}$ Auger transition (LMM_2) were found [57]. In addition, some other LMM Auger lines with $2s$ and $3s$ orbitals in the initial or final states were found in the region. The 190–200 eV region includes the $2p^{-2} \rightarrow 2p^{-1}3s^{-1}3p^{-1}$ Auger line [57].

For the photon energy region below the $1s$ threshold, the Auger electron spectrum resulting from the $1s \rightarrow np$ resonant excitations was seen. At around 3203.5 eV [50] photon energy, the Auger lines become most intense, due to the strong $1s \rightarrow 4p$ resonant photoexcitation.

Figure 2 shows the Auger electron spectra measured at photon energies 3202.0, 3206.3, 3206.5, 3209.3 eV (excess photon energies $E_{\text{exc}} = -4.3, 0, 0.2, 3.0$ eV). For photoionization with photon energies lower than the excitation energy of the Ar $1s^{-1}4p$ resonance, mostly Auger lines due to $2p^{-1} \rightarrow 3p^{-2}$ processes following L shell photoionization were seen. On the other hand, for photoionization with photon energies higher than the Ar $1s$ threshold ($E_{\text{exc}} = 0, 0.2, 3.0$ eV), LMM_1 , LMM_2 Auger lines as well as the $2p^{-1} \rightarrow 3p^{-2}$ ($LMM\alpha$) Auger lines were clearly seen. The nominal Auger energy position (peak position without the PCI effect) for those are already known [55,56]. The nominal Auger energy positions for some of the prominent LMM lines are indicated by vertical broken lines in Fig. 2. For all LMM Auger lines, the PCI shift very clearly increases as the incident photon energy is gradually lowered down from higher energy to threshold.

Figure 3 shows three selected Auger lines: (a) $LMM\alpha$ (nominal Auger energy position at 203.47 eV [55]), (b) LMM_1 (nominal Auger energy position at 216.22 eV [56]), (c) LMM_2 (nominal Auger energy position at 181.06 eV [56]) measured for excess energies $E_{\text{exc}} = 0, 0.2, 0.5, 1.0, 2.0, 3.0$ eV. Auger lines in Fig. 3 are shown with respect to their nominal Auger energy position. Figure 4 shows the PCI shifts (the difference between the maximum of the PCI distorted line shape and the nominal Auger energy position, as previously mentioned) for selected Auger lines. The position of the maximum value of the peaks by PCI were determined by fitting with a polynomial approximation.

For $LMM\alpha$ [Fig. 3(a)], the tailing and shift towards higher energy increases as the threshold is approached. The gradual change in the spectrum is quite similar to the case of one-step PCI process. Very close to threshold at excess energies $E_{\text{exc}} = 0$ and $E_{\text{exc}} = 0.2$ eV, a peak due to direct $2p$ photoionization appears on top of the nominal Auger energy position. For the case of the $2p$ hole formed by the initial KL fluorescence lifetime that PCI for single step LMM Auger process does not have [28]. Calculation of the $LMM\alpha$ Auger line shift has been carried out employing the semiclassical approach as described in Sec. III B. The inner-vacancy width $\Gamma_{\text{eff}} = 101$ meV was employed as the effective parameter value in the calculation.

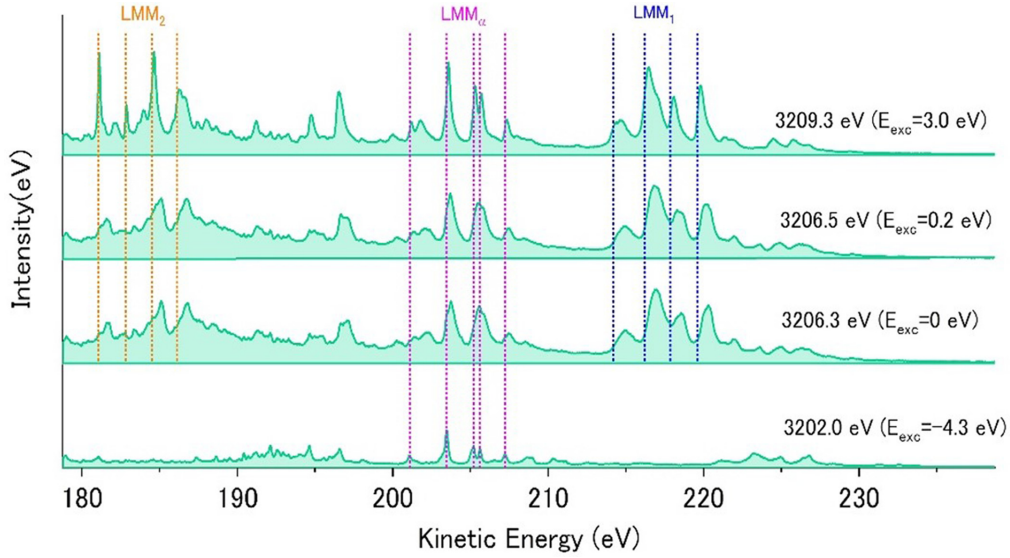


FIG. 2. Ar Auger electron spectra measured at photon energies 3202.0, 3206.3, 3206.5, 3209.3 eV (excess energies $E_{\text{exc}} = -4.3, 0, 0.2, 3.0$ eV). The vertical broken lines show the nominal Auger line positions. The kinetic energy scale along the horizontal axis is calibrated by the $L_3M_{23}M_{23}$ (1D_2) Auger line [55].

Figure 4 shows good agreement of measured and calculated shifts.

In Fig. 3(b), the PCI shift of the LMM_1 peak is seen to be larger compared to the shift of the $LMM\alpha$ peak. This is

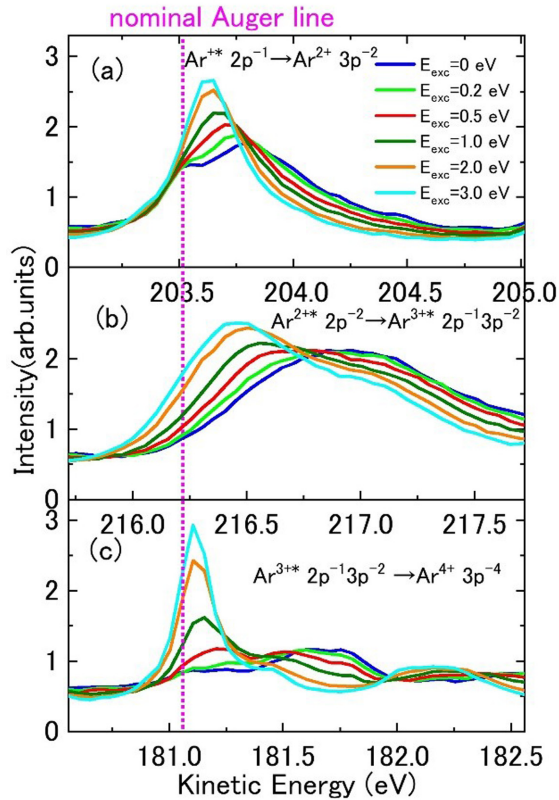


FIG. 3. The Ar Auger peaks for (a) $LMM\alpha$, (b) LMM_1 , (c) LMM_2 measured at excess energies $E_{\text{exc}} = 0, 0.2, 0.5, 1.0, 2.0, 3.0$ eV. The broken vertical line indicates the nominal Auger energy position.

the manifestation of the difference in initial-state lifetimes affecting the magnitude of the shift. The calculation of the LMM_1 Auger line shift has also been carried out with the semiclassical approach [19] which was described in Sec. III C. The values of the inner-vacancy widths Γ_1 and Γ_2 incorporated into the calculation as parameters were chosen to be $\Gamma_{1s} = 690$ meV for the initial $\text{Ar}^{++}(1s^{-1})$ ionic state and $\Gamma_{2p^2} = 240$ meV for the intermediate $\text{Ar}^{2+*}(2p^{-2})$ ionic state. The first Γ_{1s} is close to the table value [52]; the second Γ_{2p^2} one is twice $\Gamma_{2p^2} = 2\Gamma_{2p}$ than the width of the single hole state ($\Gamma_{2p} = 118$ meV [53]) and was used earlier for calculation of the PCI influence on the single KLL Auger decay in Ar [35]. The adopted value of Γ_{2p^2} is in accord with the measured value of the width of the Voigt profile of 370 meV [58]. The latter value leads to the value $\Gamma_{2p^2} = 240$ meV if one assumes

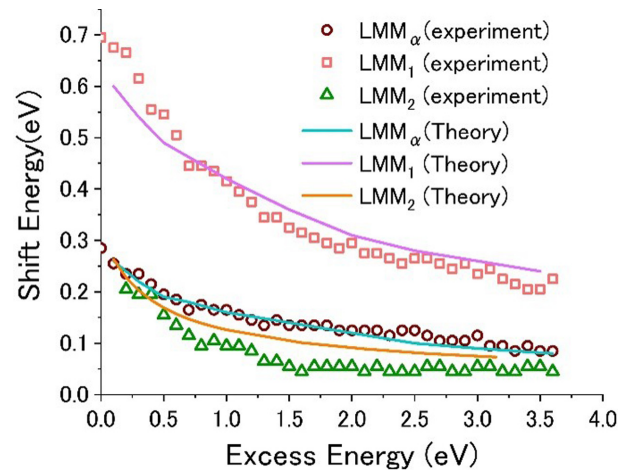


FIG. 4. The LMM Auger lines shifts are presented versus the excess photon energy ΔE above the threshold. The measurements and the calculations for the shift ε of the $LMM\alpha$, LMM_1 , and LMM_2 lines are plotted.

the electron resolution of 180 meV. The calculated values of the LMM_1 line shift agree rather well with the measured data. The considerable growth of the LMM_1 line shift observed close to the threshold comparing to the $LMM\alpha$ line is confirmed by the WKB calculation and reflects the complicated character of the PCI effect in the cascade double Auger decay. The calculated shifts agree well with the experimental values, except very close to a threshold. For LMM_1 , the shift obtained by experiment increases significantly in the region of excess energy below $E_{\text{exc}} = 0.5$ eV (Fig. 4). This could be due to the influence from the recapture of the slow photoelectron into the discrete states of the Ar^{2+} ion. For the photoelectron energy ~ 0.5 eV and the width of the $1s$ vacancy of approximately 690 meV, the distance between the outgoing photoelectron and the remaining ion is less than 10 a.u. when the $1s$ vacancy decays. The first Auger electron is very fast (near 2660 eV [35]) and leaves the interaction zone very quickly. The photoelectron feels the change in the Coulomb field of the ion and has a large probability to be recaptured into the discrete state $2p^2nl$. The second Auger electron is emitted from this state which can have a width that differs from $\Gamma_{2p^2} = 240$ meV. So, the PCI shift of the second Auger electron can differ from the case when all three electrons are in the continuum. Our calculated shift also shows an increase in this region but less than measured values. The semiclassical theory [19] for the cascade double Auger decay does not take into account the recapture of the slow photoelectron into the discrete states.

For the LMM_2 spectrum shown in Fig. 3(c), the overall tendency is that the PCI effect is smaller compared to the LMM_1 Auger spectrum [Figs. 3(b) and 4]. The measured shift of the LMM_2 Auger line ascribed to process (3) shows smaller values than the shift of the $LMM\alpha$ Auger line, although the effective width of the singly charged ion $\Gamma_{\text{eff}} = 101$ meV is less than the width of the $2p^{-1}3p^{-2}$ state, $\Gamma_{2p} = 118$ meV. This observation can be explained by the fact that when the third Auger electron is emitted the photoelectron will be located far from the ion. Therefore, the energy exchange between the photoelectron and the third Auger electron becomes smaller. An estimation carried out along the line described in Sec. III D confirms this. The estimated values of the LMM_2 shift agree reasonably with the measured data.

In all previous studies, Auger decay steps were assumed to be independent processes. No interaction between Auger electrons was considered. A very interesting aspect of PCI processes for multistep Auger decay is that the Auger electron interacts with the photoelectron which in turn interacts with the subsequent Auger electrons that follows. In other words, Auger electrons interact with one another via the photoelectron as the mediator. Throughout the process, energy conservation is maintained, so it should be instructive to plot the PCI shift of the second and subsequent Auger electrons with the horizontal axis (excess energy) shifted by the energy loss of the photoelectron due to the first PCI interaction. In Fig. 5, we plotted the peak shift of LMM_1 as a function of excess photon energy minus the PCI shift of the KLL Auger process [35]. Also, the peak shift of LMM_2 is plotted as a function of the above-mentioned effective excess energy with the peak shift of LMM_1 subtracted. Moreover, both shifts are compared to the quasiclassical theory for the case of the single Auger decay [9], and both agree to a fair extent. This shows

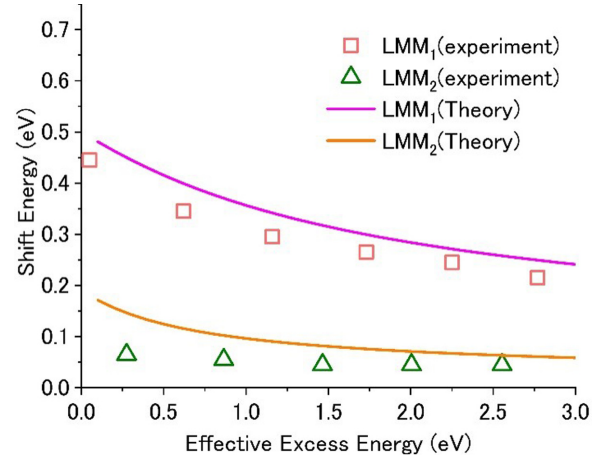


FIG. 5. PCI shift of LMM_1 and LMM_2 by effective excesses energy. (See text for details.) Both shifts are compared to the quasiclassical theory [9].

the consistency in the energy transfer among Auger electrons via interactions mediated through the common photoelectron. Future studies on various systems are called for to further elucidate the dynamics of these multielectron “billiard” type interactions among electrons transcending the “independent Auger approximation.”

V. CONCLUSION

We have examined Ar $1s$ photoionization close to threshold to study PCI occurring in the second and third steps of the multistep decay. Measurements were made close to threshold on the $2p^{-1} \rightarrow 3p^{-2}$ $LMM\alpha$ Auger spectrum following KL fluorescence, as well as the double L shell hole state following KLL Auger process leading to $2p^{-2} \rightarrow 2p^{-1}3p^{-2}$ LMM_1 Auger process and further to the $2p^{-1}3p^{-2} \rightarrow 3p^{-4}$ LMM_2 Auger transition. Each of the peaks showed clear PCI effects. The $LMM\alpha$ Auger peak after single-hole production following KL fluorescence showed shift and tailing towards higher energies similar to a one-step Auger process. The line shifts showed excellent agreement with a semiclassical calculation incorporating the effective lifetime including KL fluorescence. With the $1s^{-1} \rightarrow 2p^{-2}$ KLL Auger process as the initial step, the subsequent LMM_1 Auger transition showed some increase of shift only very close to threshold ($E_{\text{exc}} = 0-0.5$ eV). It yielded a symmetric peak shape quite different from the expectation for one-step PCI. The shift agreed well with our semiclassical PCI model. Also, for the third-step LMM_2 Auger transition, the shift increased rapidly and significantly only very close to the threshold ($E_{\text{exc}} = 0-0.5$ eV). The calculation for the LMM_2 shift agrees reasonably well with measurement. This study of the LMM Auger spectrum by photoionization of Ar $1s$ close to threshold provides significant insights into the dynamic interactions within the multistep Auger processes involving more than the previous simple picture of just one Auger electron interacting with the photoelectron and stimulates further studies, both experimental and theoretical.

ACKNOWLEDGMENTS

This material is based on work supported by the Japan Society for the Promotion of Science through Grants-in-for Scientific Research Category “C,” Grants No. 23600009

and No. 17K05600. The experiments were conducted at the GALAXIES beamline of the SOLEIL Synchrotron under Proposal No. 99170136. We are grateful to the SOLEIL staff for their operation of the facility.

-
- [1] S. Sheinerman, *J. Phys. B: At. Mol. Opt. Phys.* **27**, L571 (1994).
 [2] V. Schmidt, N. Sandner, W. Mehlhorn, M. Y. Adam, and F. Wuilleumier, *Phys. Rev. Lett.* **38**, 63 (1977).
 [3] M. Yu. Kuchiev and S. A. Sheinerman, *J. Phys. B: At. Mol. Phys.* **21**, 2027 (1988).
 [4] M. Borst and V. Schmidt, *Phys. Rev. A* **33**, 4456 (1986).
 [5] V. Schmidt, *Z. Phys. D* **2**, 275 (1986).
 [6] A. Russek and W. Mehlhorn, *J. Phys. B: At. Mol. Phys.* **19**, 911 (1986).
 [7] P. van der Straten, R. Morgenstern, and A. Niehaus, *Z Phys. D* **8**, 35 (1988).
 [8] F. Koike, *J. Phys. Soc. Jpn.* **57**, 2705 (1988).
 [9] A. Niehaus, *J. Phys. B* **10**, 1845 (1977).
 [10] F. H. Read, *J. Phys. B* **10**, L207 (1977).
 [11] A. K. Kazansky and N. M. Kabachnik, *Phys. Rev. A* **72**, 052714 (2005).
 [12] U. Hergenhahn, A. De Fanis, G. Prümper, A. K. Kazansky, N. M. Kabachnik, and K. Ueda, *J. Phys. B: At. Mol. Opt. Phys.* **38**, 2843 (2005).
 [13] S. Sheinerman, *J. Phys. B* **31**, L361 (1998).
 [14] M. Yu. Kuchiev and S. A. Sheinerman, *Sov. Phys. Usp.* **32**, 569 (1989).
 [15] G. B. Armen, *J. Phys. B* **29**, 677 (1996).
 [16] E. Shigemasa, T. Kaneyasu, Y. Tamenori, and Y. Hikosaka, *J. Electron Spectrosc. Relat. Phenom.* **156–158**, 289 (2006).
 [17] T. Gejo, T. Ikegami, K. Honma, O. Takahashi, E. Shigemasa, Y. Hikosaka, and Y. Tamenori, *J. Chem. Phys.* **140**, 214310 (2014).
 [18] M. Yu. Kuchiev and S. A. Sheinerman, *Sov. Phys. JETP* **63**, 986 (1986).
 [19] L. Gerchikov and S. Sheinerman, *Phys. Rev. A* **84**, 022503 (2011).
 [20] S. Sheinerman, P. Lablanquie, F. Penent, J. Palaudoux, J. H. D. Eland, T. Aoto, Y. Hikosaka, and K. Ito, *J. Phys. B* **39**, 1017 (2006).
 [21] R. K. Kushawaha, K. Jänkälä, T. Marchenko, G. Goldsztejn, R. Guillemin, L. Journal, D. Céolin, J. P. Rueff, A. F. Lago, R. Püttner, M. N. Piancastelli, and M. Simon, *Phys. Rev. A* **92**, 013427 (2015).
 [22] S. Sheinerman, P. Linusson, J. H. D. Eland, L. Hedin, E. Andersson, J. E. Rubensson, L. Karlsson, and R. Feifel, *Phys. Rev. A* **86**, 022515 (2012).
 [23] S. Kosugi, M. Iizawa, Y. Kawarai, Y. Kuriyama, A. L. D. Kilcoyne, F. Koike, N. Kuze, D. S. Slaughter, and Y. Azuma, *J. Phys. B* **48**, 115003 (2015).
 [24] S. Kosugi, N. Suzuki, N. Kumagai, H. Iwayama, E. Shigemasa, F. Koike, and Y. Azuma, *J. Phys. B: At. Mol. Opt. Phys.* **52**, 245002 (2019).
 [25] R. Guillemin, L. Gerchikov, S. Sheinerman, M. Zmerli, T. Marin, L. Journal, O. Travnikova, T. Marchenko, B. Lassalle-Kaiser, M. N. Piancastelli, and M. Simon, *Phys. Rev. A* **99**, 063409 (2019).
 [26] L. Gerchikov, R. Guillemin, M. Simon, and S. Sheinerman, *Phys. Rev. A* **95**, 063425 (2017).
 [27] L. Gerchikov and S. Sheinerman, *J. Phys. B* **51**, 065201 (2018).
 [28] S. Kosugi, F. Koike, M. Iizawa, M. Oura, T. Gejo, K. Tamasaku, J. R. Harries, R. Guillemin, M. N. Piancastelli, M. Simon, and Y. Azuma, *Phys. Rev. Lett.* **124**, 183001 (2020).
 [29] F. Koike, *Phys. Lett. A* **193**, 173 (1994).
 [30] F. Koike, *Nucl. Instrum. Methods Phys. Res. B* **267**, 231 (2009).
 [31] S. Kosugi, J. Martins, F. Hosseini, T. Marchenko, O. Travnikova, J. D. Bozek, K. Ito, E. Sokell, M. N. Piancastelli, M. Simon, F. Koike, and Y. Azuma, *J. Phys. B* **53**, 125001 (2020).
 [32] S. Sheinerman, P. Lablanquie, F. Penent, Y. Hikosaka, T. Kaneyasu, E. Shigemasa, and K. Ito, *J. Phys. B: At. Mol. Opt. Phys.* **43**, 115001 (2010).
 [33] P. Lablanquie, S. Sheinerman, L. Andric, J. Palaudoux, Y. Hikosaka, K. Ito, and F. Penent, *J. Electron Spectrosc. Relat. Phenom.* **185**, 198 (2012).
 [34] R. Guillemin, S. Sheinerman, C. Bomme, L. Journal, T. Marin, T. Marchenko, R. K. Kushawaha, N. Trcera, M. N. Piancastelli, and M. Simon, *Phys. Rev. Lett.* **109**, 013001 (2012).
 [35] R. Guillemin, S. Sheinerman, R. Püttner, T. Marchenko, G. Goldsztejn, L. Journal, R. K. Kushawaha, D. Céolin, M. N. Piancastelli, and M. Simon, *Phys. Rev. A* **92**, 012503 (2015).
 [36] T. Hayaishi, E. Murakami, Y. Morioka, E. Shigemasa, A. Yagishita, and F. Koike, *J. Phys. B* **27**, L115 (1994).
 [37] U. Arp, T. LeBrun, S. H. Southworth, M. A. MacDonald, and M. Jung, *Phys. Rev. A* **55**, 4273 (1997).
 [38] T. Hayaishi, E. Murakami, A. Yagishita, F. Koike, Y. Morioka, and J. E. Hansen, *J. Phys. B* **21**, 3203 (1988).
 [39] T. Hayaishi, A. Yagishita, E. Shigemasa, E. Murakami, and Y. Morioka, *J. Phys. B* **23**, 4431 (1990).
 [40] T. Hayaishi, T. Tanaka, H. Yoshii, E. Murakami, E. Shigemasa, A. Yagishita, F. Koike, and Y. Morioka, *J. Phys. B* **32**, 1507 (1999).
 [41] T. Hayaishi, Y. Fujita, M. Izumisawa, T. Tanaka, E. Murakami, E. Shigemasa, A. Yagishita, and Y. Morioka, *J. Phys. B* **33**, 37 (2000).
 [42] T. Hayaishi, T. Matsui, H. Yoshii, A. Higurashi, E. Murakami, A. Yagishita, T. Aoto, T. Onuma, and Y. Morioka, *J. Phys. B* **35**, 141 (2002).
 [43] H. Kjeldsen, T. D. Thomas, P. Lablanquie, M. Lavollée, J. H. D. Eland, F. Penent, M. Hochlaf, and R. I. Hall, *J. Phys. B* **29**, 1689 (1996).
 [44] T. Matsui, H. Yoshii, A. Higurashi, E. Murakami, T. Aoto, T. Onuma, Y. Morioka, A. Yagishita, and T. Hayaishi, *J. Phys. B* **35**, 3069 (2002).
 [45] P. Lablanquie, S. Sheinerman, F. Penent, R. I. Hall, M. Ahmad, Y. Hikosaka, and K. Ito, *Phys. Rev. Lett.* **87**, 053001 (2001).

- [46] P. Lablanquie, S. Sheinerman, F. Penent, R. I. Hall, M. Ahmad, T. Aoto, Y. Hikosaka, and K. Ito, *J. Phys. B* **35**, 3265 (2002).
- [47] C. Bomme, R. Guillemin, S. Sheinerman, T. Morin, L. Journal, T. Marchenko, R. K. Kushawaha, N. Trcera, M. N. Piancastelli, and M. Simon, *J. Phys. B* **46**, 215101 (2013).
- [48] J.-P. Rueff *et al.*, *J. Synchrotron Radiat.* **22**, 175 (2015).
- [49] D. Céolin *et al.*, *J. Electron Spectrosc. Relat. Phenom.* **190**, 188 (2013).
- [50] J. Doppelfeld, N. Anders, B. Esser, F. von Busch, H. Scherer, and S. Zinz, *J. Phys. B* **26**, 445 (1993).
- [51] U. Alkemper, J. Doppelfeld, and F. von Busch, *Phys. Rev. A* **56**, 2741 (1997).
- [52] M. O. Krause, *J. Phys. Chem. Ref. Data* **8**, 307 (1979).
- [53] M. Jurvansuu, A. Kivimäki, and S. Aksela, *Phys. Rev. A* **64**, 012502 (2001).
- [54] J. C. Levin, C. Biedermann, N. Keller, L. Liljeby, O. C.-S., R. T. Short, I. A. Sellin, and D. W. Lindle, *Phys. Rev. Lett.* **65**, 988 (1990).
- [55] L. O. Werme, T. Bergmark, and K. Siegbahn, *Phys. Scr.* **8**, 149 (1973).
- [56] F. von Busch, U. Kuetgens, J. Doppelfeld, and S. Fritzsche, *Phys. Rev. A* **59**, 2030 (1999).
- [57] R. Guillemin, K. Jänkälä, B. Cunha de Miranda, T. Marin, L. Journal, T. Marchenko, O. Travnikova, G. Goldsztejn, I. Ismail, R. Püttner, D. Céolin, B. Lassalle-Kaiser, M. N. Piancastelli, and M. Simon, *Phys. Rev. A* **97**, 013418 (2018).
- [58] M. Žitnik, R. Püttner, G. Goldsztejn, K. Bučar, M. Kavčič, T. Marchenko, A. Mihelič, R. Guillemin, L. Journal, O. Travnikova, D. Céolin, M. N. Piancastelli, and M. Simon, *Phys. Rev. A* **93**, 021401(R) (2016).